Volume 52
Number 46
14 December 2023
Pages 17045-17584

Dalton Transactions

An international journal of inorganic chemistry

rsc.li/dalton

ISSN 1477-9226

ROYAL SOCIETY OF CHEMISTRY

PAPER

M. Elena Olmos, José M. López-de-Luzuriaga *et al.*
Vapochromic behaviour of a gold(I)–lead(II) complex as a VOC sensor

Dalton Transactions

ROYAL SOCIETY OF CHEMISTRY

PAPER

View Article Online
View Journal | View Issue

Check for updates

Cite this: *Dalton Trans.*, 2023, **52**, 17119

Vapochromic behaviour of a gold(I)–lead(II) complex as a VOC sensor†

Sonia Moreno, David Royo, Abdel G. El-Hachimi, María Rodríguez-Castillo, Miguel Monge, M. Elena Olmos * and José M. López-de-Luzuriaga *

Received 27th June 2023,
Accepted 21st September 2023

DOI: 10.1039/d3dt02000b

rsc.li/dalton

The reaction among $[Au_2Ag_2(C_6F_5)_4(OEt_2)_2]_n$, $PbCl_2$ and terpyridine leads to the polymeric complex $[\{Au(C_6F_5)_2\}_2\{Pb(terpy)\}]_n$ (**1**). Its crystal structure reveals potential voids close to the lead centres large enough to hold different molecules. The availability of these free sites allows complex **1** to act as a VOC sensor. Thus, when **1** is exposed to different solvent vapours such as acetonitrile, toluene or THF, variations in its solid appearance and its photophysical properties are observed as a consequence of the formation of the new polymorphs $[\{Au(C_6F_5)_2\}_2\{Pb(terpy)(CH_3CN)_2\}]_n$ (**2**), $[\{Au(C_6F_5)_2\}_2\{Pb(terpy)\}]_n$·Tol (**3**) and $[\{Au(C_6F_5)_2\}_2\{Pb(terpy)(THF)\}]_n$·THF (**4**). Each polymorph displays a different emission energy depending on its structure and the presence of metallophilic interactions. In addition, the reversible solvent molecule exchange allows the tuning of the luminescence emissions in the greenish yellow–red range. DFT and TD-DFT calculations were performed to explain the origin of the luminescence of all these complexes.

Introduction

During the last few years, several studies in several laboratories[1] have shown that heterometallic complexes containing Au(I) and other closed shell metal ions are responsible for interesting optical properties.[2–6] In them, it has been observed that the luminescent behaviour of the complexes is associated with the presence of different Au···M or/and Au···Au interactions in their solid state structures and also serves as an indication of the presence of these interactions even in solution.[7,8] Additionally, the number and type of ligands also influence the geometry and electronics of the metal centres and, therefore, the emissive character of the complexes.

On the other hand, McCrone defined "a solid crystalline phase of a given compound resulting from the possibility of at least two different arrangements of the molecules of that compound in the solid state" as polymorphism.[9] This situation can obviously affect the optical properties of the materials depending on the different arrangements of metals or on the interactions between them in each polymorph. One special class of polymorphism called solvatopolymorphism is present in systems where the crystal structures are defined by different unit cells that differ in their elemental composition by means of the inclusion of one or more solvent molecules.[10]

The presence of solvent molecules in the crystal packing should not affect the optical behaviour whether there is no metal···solvent interaction (neither increasing their coordination numbers nor varying their geometries) or even if they exist when they do not influence the strength of the intermetallic interactions or other weak noncovalent bonds, including hydrogen bonds, π-stacking or van der Waals interactions;[11] nevertheless, the introduction of these molecules into the network as solvation molecules in solution or as vapours frequently leads to important modifications in the crystal packing, producing changes in these interactions and, as a consequence, in their colours, which are often perceptible to the human eye, and even deeper under UV light. This situation is particularly interesting since these can find application as smart materials such as gas sensors and optical fibre sensors for volatile organic compound detection.

Although in the last few years there has been an increasing number of metallic complexes and materials dealing with this topic, especially in the case of gold-containing compounds, they offer a poorly explored, but fertile area of work, based on the facility of drawing together gold atoms to sub-van der Waals distances in their complexes, interactions that are strongly influenced by the environment and that greatly modify the photophysical properties of the aggregates. This was, for instance, the case of the pioneering well-known Eisenberg's dithiocarbamate gold(I) complex $[Au(S_2CN(C_5H_{11})_2)]_2$, in which the presence of polar aprotic solvents causes its polymerization through Au···Au contacts between

Departamento de Química, Universidad de La Rioja, Centro de Investigación en Síntesis Química (CISQ), Complejo Científico-Tecnológico, 26006 – Logroño, Spain. E-mail: josemaria.lopez@unirioja.es, m-elena.olmos@unirioja.es

† Electronic supplementary information (ESI) available: Spectroscopic characterization, structural characterization, powder X-ray diffraction analysis, and computational studies. CCDC 2266131–2266133. For ESI and crystallographic data in CIF or other electronic format see DOI: https://doi.org/10.1039/d3dt02000b

dimers, being completely reversible by drying.[12] Since then, a number of reports on this topic have been published,[13,14] but most of the complexes described show this behaviour in an irreversible way, or exclusively for one specific solvent/vapour. A few reports described complexes sensitive to several vapours and these, at the same time, show reversibility under mild conditions. This is the case of the heteronuclear gold–copper complex described by Koshevoy *et al.* in which up to four different crystalline forms are obtained when the alkynyl complex $[Au_2Cu_2(C_2OHC_5H_8)_4]_n$ is crystallized from methanol; ethanol, acetone or chloroform; toluene; and diethyl ether or ethyl acetate solutions, each polymorph showing different photoluminescence characteristics and some of them being interconvertible upon exposure to vapours of other solvents.[13a]

In spite of the interest that this research is attracting, there are still many questions to respond and more examples are needed to try to rationalize the mechanisms of this behaviour. In fact, the exhaustive control of polymorph formation has been recognized as an important aim for the production of functional solid materials.

With regard to our ongoing studies on the optical properties associated with heteronuclear gold–heterometal materials, one of the main goals is the analysis of the influence of external stimuli on their optical behaviour. In our case, we have contributed with several examples of this type of behaviour in heteronuclear complexes. Thus, for instance, the mixed gold(I)–thallium(I) complex $[AuTl(C_6Cl_5)_2]_n$, reported by some of us,[13b,c] reacts with different volatile organic compounds that covalently bond to the thallium centres, which produces visible changes that are completely reversible by moderate heating at 100 °C. Other examples are those of a series of gold(I)–silver(I) derivatives of stoichiometry $[Au_2Ag_2(C_6X_5)_2L_2]_n$ (X = halogen; L = neutral ligand),[13d–f] in which reversible or irreversible conversions were dependent on the donor affinity of the different vapours to silver and the nature of the perhalophenyl ligands.

In addition, we have recently contributed a number of works in which we analyse the optical properties of heterometallic complexes showing Au(I)···Pb(II) interactions.[15] The number of reported complexes that present Au(I)···Pb(II) interactions is very scarce and, in particular, studies on the influence of external stimuli, such as vapours, solvents, temperature or pressure, on these derivatives have not been published so far.

Therefore, we focused our efforts on this last field of research, and in this paper we report the synthesis, structural characterization, reversible response to solvents and their vapours as well as a computational study of the complex $[\{Au(C_6F_5)_2\}_2\{Pb(terpy)\}]_n$ (**1**) and its four solvatopolymorphs containing acetonitrile (**2**), toluene (**3**), tetrahydrofuran (**4**) or benzonitrile (**5**).

Results and discussion

Synthesis and characterization

Complex $[\{Au(C_6F_5)_2\}_2\{Pb(terpy)\}]_n$ (**1**) was prepared according to the literature procedure.[16] Complex **1** was obtained by reaction of the heterometallic polymer $[Au_2Ag_2(C_6F_5)_4(OEt_2)_2]_n$ with $PbCl_2$ and terpyridine in a 2 : 1 : 1 (Au : Pb : Terpy) molar ratio, using methanol as the solvent. Complex **1** is stable to air and moisture for long periods. It is soluble in MeOH and slightly soluble in most common organic solvents such as dichloromethane, acetonitrile, toluene, THF or benzonitrile, but insoluble in diethyl ether or *n*-hexane.

Treatment of complex **1** with solvents with different donor abilities leads to new heterometallic Au(I)–Pb(II) complexes displaying the same Au–Pb–Au metallic sequence, but a new coordination environment for the Pb(II) atom. Thus, the addition of acetonitrile, toluene, tetrahydrofuran or benzonitrile gives rise to polymorphs **2–5**, respectively (Scheme 1), the latter recently published by us.[17] By contrast, solvents and vapours such as diethyl ether and *n*-hexane, wherein the complex is not soluble, do not provoke detectable changes in it.

All the analytical and spectroscopic data of the new complexes agree with the proposed stoichiometries. Thus, for all complexes, the IR spectra show, among others, the absorption bands related to the presence of the $[Au(C_6F_5)_2]^-$ units close to 1505, 955 and 770 cm^{-1} and those due to the ν(C≡N) stretching vibrations arising from the terpy ligand, appearing around 1590 cm^{-1}. In the case of polymorph **2**, an additional band associated with the ν(C≡N) stretching vibrations from the acetonitrile molecules is observed at 2247 (**2**) cm^{-1} (Fig. S2–S4†).

The molar conductivity measurements of complexes **2–4** in acetone show values corresponding to the 2 : 1 electrolyte, suggesting complete dissociation of their ionic counterparts, two $[Au(C_6F_5)_2]^-$ anions and a $[Pb(terpy)]^{2+}$ cation, and the loss

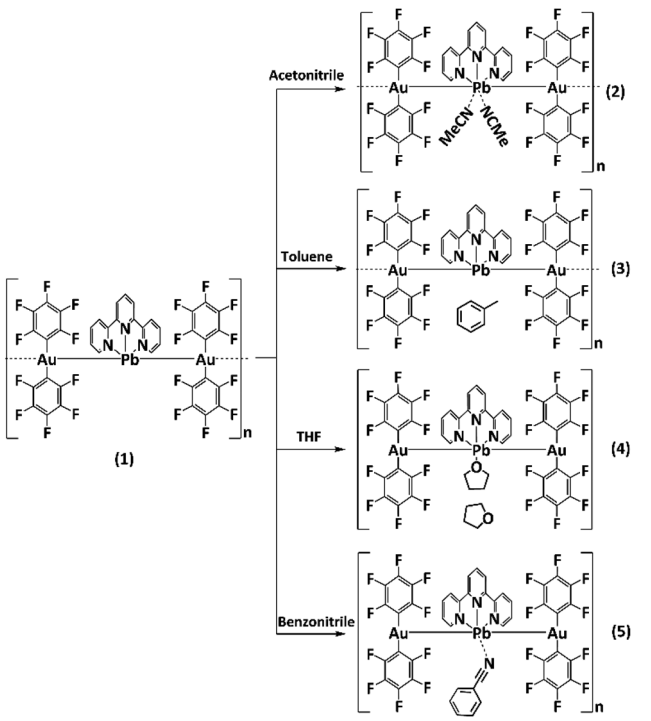

Scheme 1 Syntheses of complexes **2–5**.

of the metallophilic interactions in solution, in a similar way that has been described for **1**[16] and **5**.[17]

Regarding their MALDI(−) mass spectra, they show a peak corresponding to the $[Au(C_6F_5)_2]^-$ unit at m/z = 530, and in their MALDI(+) mass spectra a peak corresponding to the $[\{Au(C_6F_5)_2\}\{Pb(terpy)\}]^+$ fragment is detected at m/z = 972.

The ^{1}H NMR spectra of all complexes in [D$_6$]-DMSO show six signals corresponding to the terpyridine ligand in the range 8.76–7.47 ppm. In addition, the signals related to solvent molecules are also observed (Fig. S5–S7†).

Finally, the ^{19}F NMR spectra of complexes **2–4** (Fig. S8–S10†) display signals corresponding to the C_6F_5 groups bonded to gold(I) at −114.6 (m, F_o), −161.5/−161.7 (t, F_p) and −162.8/−163.0 (m, F_m) ppm, with chemical shifts very similar to those of the precursor $NBu_4[Au(C_6F_5)_2]$, suggesting the rupture of the Au···Pb metallophilic interactions in solution.

X-ray crystal structure determination

The crystal structure of complex **1** has been previously described in the literature.[16] However, it will be also commented on in this work for comparative purposes. An in-depth study of the 3D structural arrangement of complex **1** revealed the presence of empty channels that run parallel to the crystallographic *y* axis with interatom distances of around 3.765 Å (Fig. 1) and diameters close to 17.6 Å, which are large enough to accommodate small molecules. In fact, the slow evaporation of acetonitrile, toluene or tetrahydrofuran solutions of complex **1** leads to the growth of single crystals adequate for their study by X-ray diffraction techniques revealing the filling of the empty channels by solvent molecules.

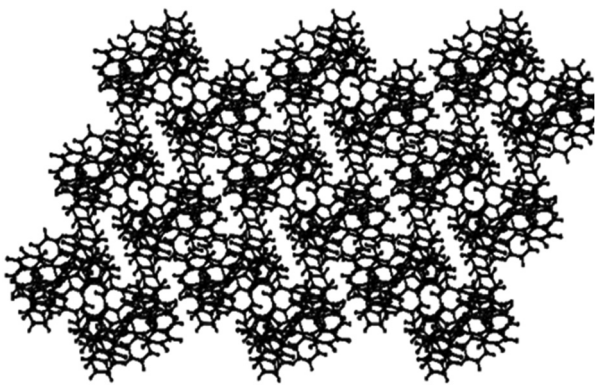

Fig. 1 Crystal structure of **1** viewed down the crystallographic *y* axis.

Compounds **2–5** display a similar structural arrangement concerning the trinuclear $[\{Au(C_6F_5)_2\}\{Pb(terpy)\}\{Au(C_6F_5)_2\}]$ building blocks. The X-ray structure of complex **5** has been previously reported;[17] but it is briefly discussed for comparative purposes. Both gold(I) atoms within the trinuclear Au_2Pb unit are linearly coordinated to two pentafluorophenyl groups with an additional (and rather uncommon) Au···Pb metallophilic interaction. These heterometallic interactions are quite similar for all the complexes with Au–Pb distances of 2.8964(5)–2.9670(5) (**1**), 2.9740(5)–2.9825(5) (**2**), 2.8470(14) and 2.8856(9) (**3**), 2.9262(3) and 2.9645(3) Å (**4**), and 2.8349(4) and 2.8646(4) Å (**5**). These Au–Pb distances compare well with those found in the decanuclear Au_6Pb_4 complex $[\{Au(C_6F_5)_2\}_6\{PbCl(terpy)\}_2\{Pb(terpy)\}_2]$ where the atom *trans* to gold is another gold centre (2.8776(9)–2.9332(9) Å),[16] and to those observed for $[Au_2Pb(CH_2P(S)Ph_2)_4]$ (2.896(1) and 2.963(2) Å),[18] in which the Au···Pb contacts are supported by the P,S-donor bridging ligands. In contrast, the Au–Pb distances are longer when the atom *trans* to gold is chlorine, as observed in the related compounds $[\{Au(C_6F_5)_2\}_6\{PbCl(terpy)\}_2\{Pb(terpy)\}_2]$ (3.2719(9); 3.2183(9) Å) and $[\{Au(C_6F_5)_2\}\{PbCl(terpy)\}]$ (3.2957(6) Å).[16]

With the only exception of compound **4**, this trinuclear Au_2Pb units are held together through aurophilic interactions of different strengths [Au–Au distances of 3.1315(5) and 3.3060(5) Å in **1**; 3.3626(7), 3.4345(7) and 3.5413(7) Å in **2**; 2.9309(13) Å in **3**, and 2.8920(5) Å in **5**], thus forming polymeric chains (Fig. 2). In contrast, in the case of **4**, the shortest Au–Au distance (5.818 Å) is too long to consider any kind of aurophilic interaction;[19] therefore, the crystal structure of complex **4** can be considered as formed by discrete molecules (Fig. 3).

In all the cases, the intermetallic contacts are reinforced by π–π interactions of different strengths that appear between pentafluorophenyl groups and/or between aromatic rings of perhalophenyl and terpyridine ligands, all of them with

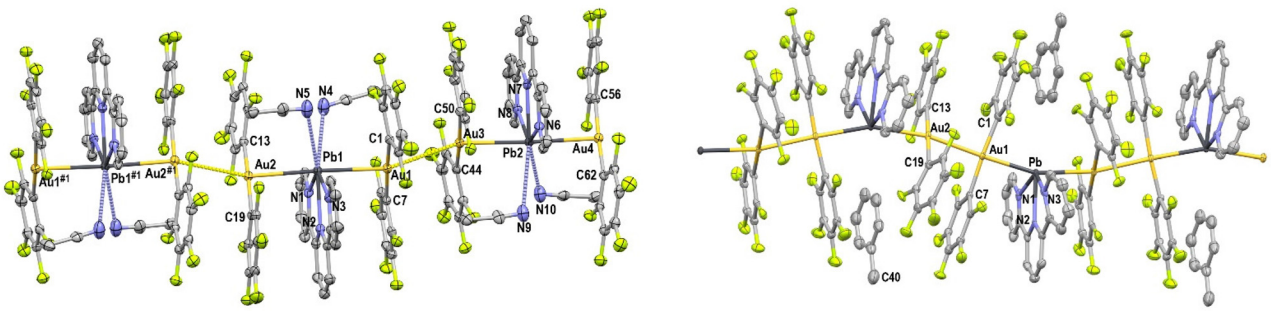

Fig. 2 Crystal structures of complexes **2** (left) and **3** (right). Selected bond lengths (Å) and angles (°) of complex **2**: Au(1)–Pb = 2.9827(5), Au(2)–Pb = 2.9781(5), Au(1)–Au(1)$^{\#1}$ = 3.4343(5), Au(2)–Au(2)$^{\#1}$ = 3.3620(7), Pb–N(3) = 3.314, Au(1)–Pb–Au(2) = 177.251(15), Pb–Au(2)–Au(2)$^{\#1}$ = 158.693(19). Selected bond lengths (Å) and angles (°) of complex **3**: Au(1)–Pb = 2.8446(15), Au(2)–Pb = 2.8878(11), Au(1)–Au(2) = 2.9315(15), Au(1)–Pb–Au(2) = 160.21(4), Pb–Au(2)–Au(1) = 176.98(5).

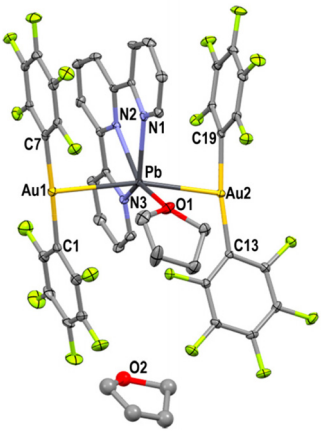

Fig. 3 Crystal structure of complex **4**. Selected bond lengths (Å) and angles (°): Au(1)–Pb = 2.9645(3), Au(2)–Pb = 2.9263(3), Pb–O = 2.787, and Au(1)–Pb–Au(2) = 163.965(7).

centroid–centroid distances within the range of π-stacking interactions.[20]

The lead atom within each trinuclear Au_2Pb unit, in addition to displaying two Pb···Au metallophilic interactions, is symmetrically coordinated to the three nitrogen atoms of a terpy ligand with Pb–N bond lengths in the ranges of 2.490(7)–2.548(7) Å in **2**, 2.457(14)–2.488(19) Å in **3**, and 2.514(3)–2.566(3) Å in **4**, with longer distances found in the non-polymeric complex **4**. All these values are similar to those found in **1** (2.451(6)–2.526(6) Å) and **5** (2.450(7)–2.532(11) Å), and lie within the usual values found for hemidirected Pb(II) complexes[21] containing terpy or terpyridine-type ligands.[22]

One of the main structural differences among the polymorphs described in this study is found in the inclusion of solvent molecules to **1**, which can either be incorporated into the coordination sphere of Pb(II) or stay in its immediate surroundings. Thus, for complex **2**, two acetonitrile molecules are weakly connected to each lead(II) centre with dissimilar Pb–N distances of 3.256(1) and 3.538(1) Å, generating a distorted pentagonal bipyramid environment for the lead atom, in which the inert pair is stereochemically inactive, with the gold centres in the apical positions (Fig. 2 left and S11†). On the other hand, complex **3** incorporates a toluene molecule per trinuclear unit, which is only interconnected through C–H···F hydrogen bonds (Fig. S12†), while no π–π interactions are found between the solvent and the aromatic rings present in the heterometallic compound. In the structure of polymorph **4**, two THF molecules are present per trinuclear unit, but while one of them is bonded to the lead(II) atom (Pb–O = 2.786(3) Å), the second one just acts as a crystallization solvent molecule (Fig. 3 and S13†). Finally, complex **5**, as previously discussed in detail in the literature,[17] displays one disordered benzonitrile molecule per trinuclear fragment with a different percentage of coordinated and non-coordinated solvent molecules depending on the external pressure or temperature.

On the other hand, the differences found in the Au–Pb–Au and Au–Au–Pb angles within the heterometallic chains of the

Fig. 4 Metallic chain skeleton of compounds **2** (up), **3** (centre) and **5** (bottom). Colour codes: gold: yellow; lead: dark grey.

solvate-containing compounds **2–5** are also worth noting (Fig. 4). Thus, the Au–Au–Pb angles in **3** and **5** are approximately linear (168.07(4) and 176.93(4)° in **3**, and 170.13(1) and 175.66(1)° in **5**), while the Au–Pb–Au angles in the structures of compounds **3–5** are narrower (160.26(3)° in **3**, 164.0(1)° in **4**, and 156.87(2)° in **5**). In contrast, an opposite trend is found in the crystal structure of complex **2**, which shows Au–Au–Pb angles in the range 155.64(2)–158.70(2)°, and values of 177.26(1) and 177.53(1)° for the Au–Pb–Au angles, that is, the lead atoms are closer to linearity than the gold ones in the case of **2**.

Optical properties

Absorption in solution and in the solid state. As shown in Fig. 5, the absorption spectra of complexes **2–5** in DMSO solutions are quite similar. Thus, they display one band at 263 nm ($\varepsilon = 2.8 \times 10^4$ (**2**), 3.0×10^4 (**3**), 3.1×10^4 (**4**) and 2.7×10^4 M^{-1} cm^{-1} (**5**)) corresponding to the gold precursor $NBu_4[Au(C_6F_5)_2]$, so it is likely to arise from internal $\pi \rightarrow \pi^*$ transitions located between the π orbitals of the perhalophenyl groups. A second band appears in all the spectra at 280 nm ($\varepsilon = 2.0 \times 10^4$ (**2**), 2.2×10^4 (**3**), 2.4×10^4 (**4**) and 2.1×10^4 M^{-1} cm^{-1} (**5**)), which corresponds to the terpyridine ligand, so it is assigned to $\pi \rightarrow \pi^*$ transitions located in aromatic rings. Finally, there is a last common band at 335 nm ($\varepsilon = 1.5 \times 10^3$ (**2**), 1.8×10^3 (**3**),

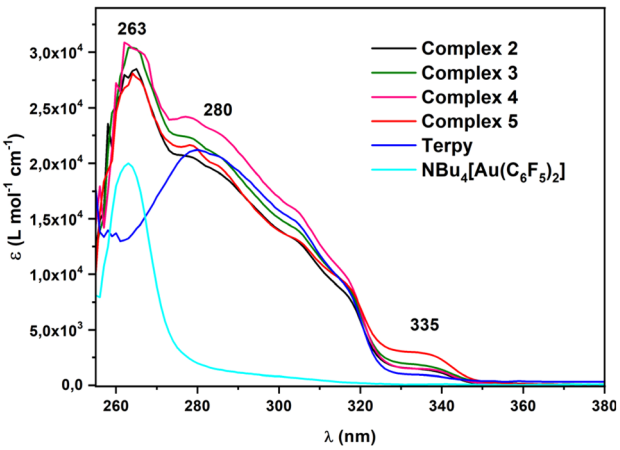

Fig. 5 UV-vis absorption spectra of compounds **2–5**, the gold(I) precursor $NBu_4[Au(C_6F_5)_2]$ and the terpyridine ligand in DMSO.

1.5×10^3 (**4**) and 2.9×10^3 M^{-1} cm^{-1} (**5**)), which also appears in the spectrum of the free terpyridine ligand, so it could be assigned to $\pi \rightarrow \pi^*$ transitions located in rings of the ligand.

In summary, due to dissociation in solution, the spectra of all the complexes are similar and can be considered the sum of the Au precursor and the terpy ligand.

On the other hand, their solid-state absorption spectra (Fig. 6) display interesting features, because, in addition to a strong and wide absorption band between 260 and 350 nm, a lower energy absorption also appears. Besides, the absorption spectra corresponding to the gold(I) precursor $NBu_4[Au(C_6F_5)_2]$ and to the terpyridine ligand show no absorption at similar values, which seems to indicate that these transitions are influenced by the gold–gold or gold–lead interactions.

This is in accordance with the shift of the lower energy band depending on the strength of the metallophilic interactions observed in their crystal structures. Thus, in the spectrum of **5**, which shows the shortest Au–Au and Au–Pb distances, this absorption is located at the longest wavelength.

Luminescence. All the compounds display an intense luminescence in the solid state at room temperature and at 77 K (Fig. 7 and 8). In contrast, all of them are non-luminescent in solution, probably due to the rupture of the metal–metal interactions by the solvent. This fact agrees with the absorption spectra in solution, as well as with the molar conductivity values and MALDI mass spectra measurements (Experimental section).

By contrast, the excitation spectra resemble those of the absorption spectra in the solid state, indicating that these absorptions give rise to the observed emissions. Thus, in the solid state at room temperature, complex **2** shows a greenish yellow luminescence with an emission band maximum at 550 nm upon excitation at 460 nm. Complexes **3** and **5** exhibit a dark red luminescence almost imperceptible to the human eye because it is at the limit of the UV region, due to emission maximum bands at 770 (**3**) and 780 (**5**) nm (excitation at 670 (**3**) and 725 (**5**) nm). The remaining complex with the O-donor solvent (**4**) shows the greatest displacement with respect to compound **1**, with very intense green luminescence with an emission band at 530 nm upon excitation at 320 or 400 nm.

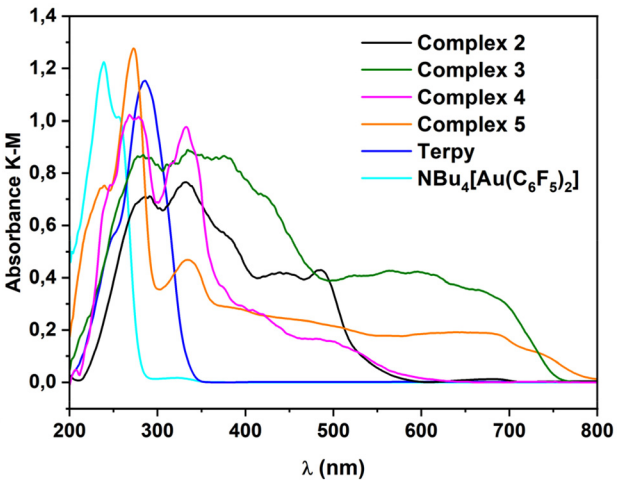

Fig. 6 UV-vis absorption spectra of compounds **2–5**, the gold(I) precursor $NBu_4[Au(C_6F_5)_2]$ and the terpyridine ligand in the solid state.

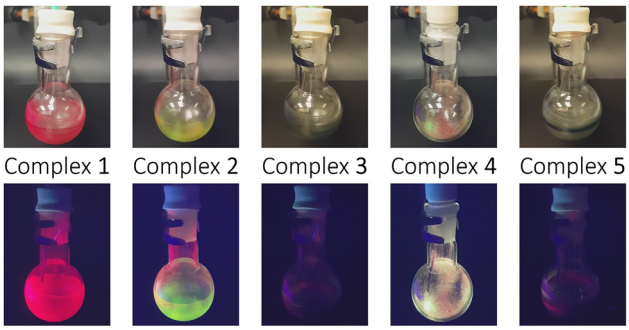

Fig. 7 Photographs of the solid colour (up) and luminescence (bottom) of compounds **1–5**.

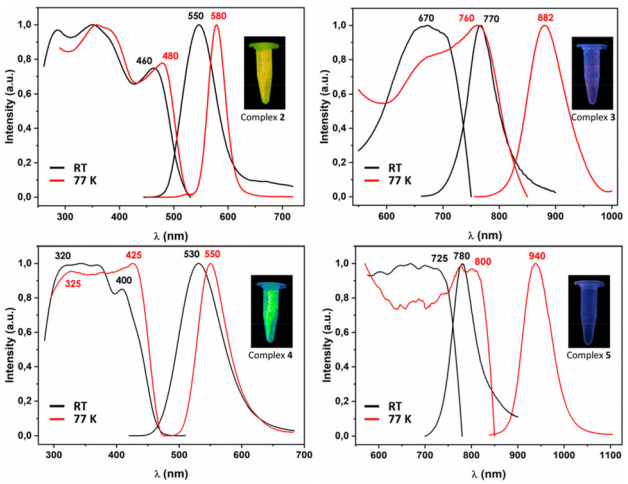

Fig. 8 Excitation and emission spectra in the solid state at room temperature (black) and 77 K (red) for complexes **2** (up, left), **3** (up, right), **4** (down, left) and **5** (down, right).

The large Stokes shifts and emission lifetime measurements both at room temperature and at 77 K in the microsecond range allow us to suggest that these transitions are based on phosphorescence processes (Fig. S29–S35†). As can be seen in Table 1, the values obtained for lifetimes at 77 K are higher than those obtained at room temperature for all compounds. Quantum yield measurements of complexes **2–5** in the solid state at room temperature exhibit different emission quantum yields with values of 43 (**2**), 26 (**3**), 98 (**4**) and 25% (**5**).

Finally, at 77 K, the emission bands shift to lower energies in all the cases. The red emission shifts observed at 77 K are common in heteronuclear derivatives displaying unsupported intermetallic interactions, in which the metallic centres are involved in the transitions responsible for the emissive properties. This has been repeatedly justified as a consequence of the thermal contraction of the structure at 77 K that reduces

Table 1 Photophysical properties of compounds **2–5** in the solid state

Complex	**2**	**3**	**4**	**5**
τ (μs) (RT)	0.853	0.226	2.592	0.286
τ (μs) (77 K)	1.214	1.734	4.021	—
Φ (%, RT)	43	26	98	25

the metal–metal distances and, hence, the HOMO–LUMO gap. Thus, complex **2** exhibits a shift in its emission band from 550 nm (excitation at 460 nm) to 580 nm (excitation at 480 nm); complexes **3** and **5** show an infrared emission band at 882 or 940 nm (770 or 780 nm at RT), respectively, upon excitation at 760 (**3**) or 800 nm (**5**). Finally, the emission band in complex **4** shifts from 530 (excitation at 320 or 400 nm) to 550 nm (excitation at 325 or 425 nm) when lowering the temperature.

Reversible vapochromism among the complexes. Interestingly, compounds **2–5** undergo an immediate colour and luminescence transformation, reverting to compound **1** after being subjected to methanol vapours, thus exhibiting a vapochromic behavior (Fig. S14†)

The powder diffraction patterns of derivatives **2–5** differ from that obtained for starting compound **1** (Fig. S15–S19†), indicating the complete insertion of the VOCs into the complex, whether coordinated or not, unequivocally confirming the ability of **1** to react in the solid–gas phase with these solvents when acting as VOCs, and demonstrating that a change in the structure of the complex occurs.

Therefore, we carried out an X-ray powder diffraction study in order to analyse the reversibility of the exchange process of five different solvents (methanol, acetonitrile, toluene, tetrahydrofuran and benzonitrile) when compound **1** is subjected to solvent vapours (Fig. S20–S28†).

Thus, upon subjecting any of these compounds to methanol vapours for a few seconds, all of them change to a reddish colour and exhibit intense red luminescence, which indicates that complete transformation into compound **1** occurs. To confirm this transformation and that it is complete, the powder X-ray diffractograms of pure compounds **2–5** were recorded and their diffraction patterns were compared with those of the same derivatives after subjecting them to methanol vapours, as well as with the diffraction pattern of compound **1** (Fig. S21–S24†).

In addition, exposure of compounds **2–5** to air for a not very long period of time leads to the loss of the previously incorporated solvents, all of them regenerating the starting derivative **1**. This process can be accelerated by the application of manual pressure in a mortar, achieving the total change in a few seconds, as confirmed by the X-ray powder diffractograms of these three compounds before and after being subjected to pressure and their comparison with that of the precursor **1**.

Finally, it should be noted that any of these compounds can be interconverted into one another without going through compound **1**. Thus, if any of compounds **2–5** are subjected to acetonitrile, toluene, THF or benzonitrile vapours, they displace the previous solvent, becoming another pseudopolymorph, thus demonstrating in all cases the possibility of interconversion that these derivatives have. In summary, with a single solid of any of them, the rest of the compounds can be obtained by simple exposition to vapours of the adequate solvent.

In the case of exposure to acetonitrile vapours, a mixture of **2** and precursor compound **1** is observed in all cases since, as discussed above, this compound is not stable in air for long periods of time, gradually losing solvent and reverting to the starting complex **1**.

Computational studies

DFT and TD-DFT computational calculations were carried out to elucidate the origin of the photophysical properties displayed by all the complexes in the solid state. Models **2a–4a** were chosen based on the crystal structures of complexes **2–4**, representing the most important interactions. Model systems were built up considering two equal Au_2Pb units linked through an unsupported gold(I)···gold(I) contact to study this type of interaction, except for complex **4**, in which this intermetallic distance is too large (Fig. S36†).

The electronic structures of the three models (**2a–4a**) were computed through dispersion-corrected single point DFT calculations. For the models displaying the same Au_2Pb trinuclear core disposition (**2a** and **3a**), the HOMOs are mainly placed at the metal centres, largely at gold atoms and to a lesser extent at the lead atoms, with a minor contribution from the perhalophenyl groups (Fig. 9 and 10 and Tables S2 and S3†). On the other hand, the LUMOs calculated for all models appear to be mostly located at the terpy ligand and display a π^* character, indicating that terpy has a highly relevant role in the luminescent behavior of these complexes, being involved in metal to ligand charge transfer (MLCT) transitions.

In the case of model **4a**, in which aurophilic interactions are not present, the computed electronic structure provides a different arrangement of molecular orbitals. The HOMO is now placed at the neighbouring perhalophenyl groups, and the LUMO is located at the terpy ligand (Fig. 11 and

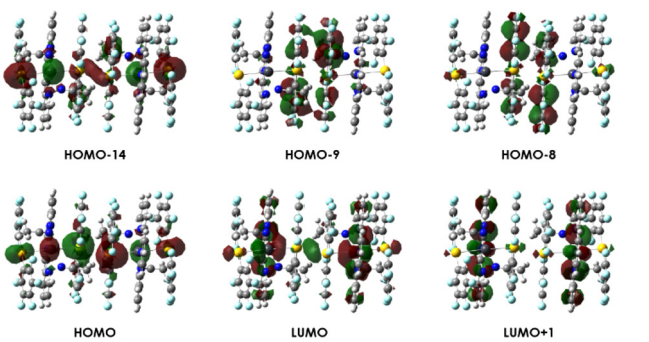

Fig. 9 Molecular orbitals involved in the most important transitions calculated for model $[\{Au(C_6F_5)_2\}_2\{Pb(terpy)(NCMe)_2\}]_2$ **2a**.

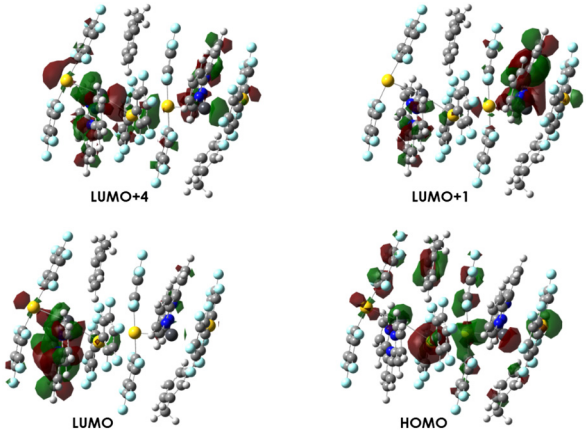

Fig. 10 Molecular orbitals involved in the most important transitions calculated for model $\{[\{Au(C_6F_5)_2\}_2\{Pb(terpy)\}]\cdot toluene\}_2$ **3a**.

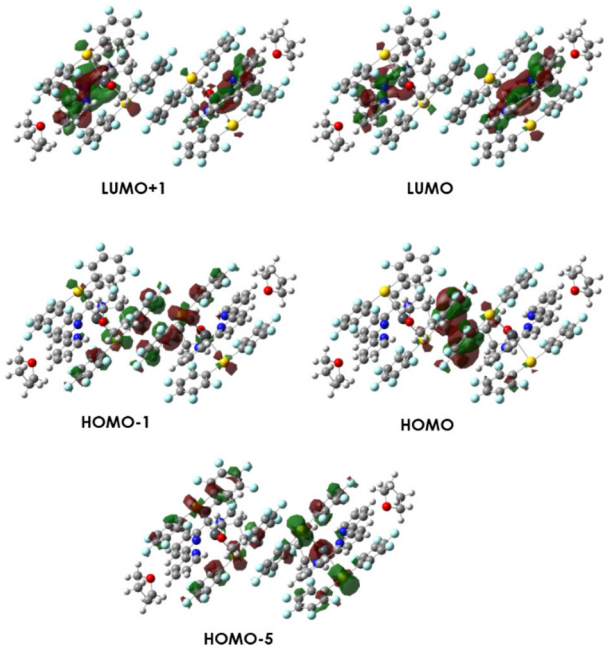

Fig. 11 Molecular orbitals involved in the most important transitions calculated for model $\{[\{Au(C_6F_5)_2\}_2\{Pb(terpy)(THF)\}]\cdot THF\}_2$ **4a**.

Table S4†). Therefore, for this complex, ligand-to-ligand charge transfer (LL′CT) is likely favoured upon excitation.

To confirm the origin of electronic transitions that could be related to the absorption spectra and luminescent emissions observed experimentally for the reported complexes, we performed an analysis of the energy of the most intense singlet–singlet electronic excitations computed using the TD-DFT approach. Thus, we compared these allowed transitions with the experimental UV-vis solid-state spectra of the complexes, obtaining a good match between the predicted excitations and the experimental absorption profile. Moreover, since the emissive behaviour of these complexes could arise from phosphorescence processes in view of their lifetimes, in the microsecond range, we also computed the lowest singlet–triplet excitation at the TD-DFT level for all models, and we compared the corresponding predicted energies with the experimental excitation spectra.

The computed first few singlet–singlet excitations for models **2a–3a** provide the predicted absorption spectra, which can be divided into two types of excitations: one corresponding to the HOMO–LUMO transition (at lower energy) and the rest of excitations at higher energies. The excitation calculated at 364 nm for model **2a** and at 354 nm for **3a** takes place from the HOMO to LUMO+4. The latter is located at the fragment $[Pb(terpy)]^{2+}$. For model **2a**, the electronic transition associated with singlet–singlet excitation at 351 nm occurs between HOMO−14 and LUMO+1, being quite similar to the HOMO and LUMO, centered at the metal centers and terpy ligands, respectively. In the case of model **3a**, the transition at 458 nm takes place between the HOMO and LUMO+1, centered at the terpy ligand, as well as the LUMO.

Regarding model **4a**, the lowest energy excitation is a combination of two electronic transitions: the HOMO → LUMO+1 (50%) and the HOMO−1 → LUMO (23%) transitions. On the other hand, there is another more energetic excitation at 334 nm that takes place between two electronic transitions: HOMO−9 → LUMO+3 (37%) and HOMO−19 → LUMO+1 (31%). The HOMO−19 orbital is mainly located at the terpy ligand with a minor contribution of the perhalophenyl rings. However, HOMO−9 is inverted, being mainly centered at the perhalophenyl groups. LUMO+1 and LUMO+3, as well as the LUMO, are located at the terpy ligand.

If we analyze the lowest energy excitations, the first singlet–triplet transition arises as a whole for all model systems from the HOMO to the LUMO. These computed results seem to indicate that the electronic transition responsible for the phosphorescence emission observed for all complexes could have its origin in metal to ligand (terpy) charge transfer (MLCT) transition. Besides, in the case of **4a**, there is another transition with a high contribution, which is from HOMO−1 to the LUMO. HOMO−1 is located at neighbouring perhalophenyl groups, not only at the perhalophenyl groups with π–π stacking, but also at the other perhalophenyl groups joined to the same gold(I) centres, with a small contribution from the metal centers (Fig. 11).

We also carried out periodic DFT calculations (computational details) to explore the electronic structure and the complex···solvent interaction energies (IE) of the experimentally described Au(I)–Pb(II) heterometallic complexes, bearing four different solvents namely acetonitrile (**2**), toluene (**3**), THF (**4**) or benzonitrile (**5**).

We performed an interaction energy (IE) calculation of the Au–Pb molecules using periodic boundaries. Complexes **2–5** display an explicit solvation that, as is shown experimentally, leads to a reversible process, complex **1** being the most stable species from a thermodynamic point of view. Therefore, the calculation of the IE could explain the tendency for the displacement of the solvate molecules from each supramolecular arrangement. To evaluate the IE, eqn (1) in Fig. 12 is used,

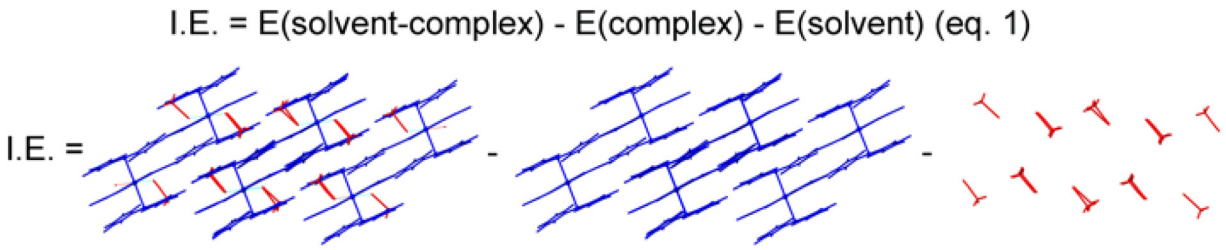

Fig. 12 Representation of the model systems used for the estimation of the interaction energy for complex **2**.

where $E_{(solvent\text{-}complex)}$, $E_{(complex)}$, and $E_{(solvent)}$ correspond to the energy of the supramolecular arrangements of complexes **2–5** interacting with the solvents, the complexes without solvent, and the explicit solvent, respectively. This qualitative approach highlights the interaction between the solid-state systems and the solvent molecules acetonitrile (**2**), toluene (**3**), tetrahydrofuran (**4**) or benzonitrile (**5**). Fig. 12 also depicts the computed periodic crystal structure of complex **2** with and without solvent molecules and the isolated explicit acetonitrile solvent. The interpretation of the solvent–complex interaction is based on two main parts: (i) the observed experimental tendency compared to the calculation results, as well as the effect caused by this interaction to make stress in the cells of the four materials, and (ii) the high tendency to lose the solvent spontaneously during the synthesis.

The computed results show that complex **2**, bearing acetonitrile molecules, displays a repulsive (positive) interaction energy value of +8.23 eV. This value reflects a clear tendency of losing solvent molecules, as observed experimentally, leading to a more thermodynamically stable empty supramolecular arrangement and free solvent molecules. In the case of the acetonitrile solvate, this is the highest interaction energy found for all systems. In addition, complex **4** bearing THF has also a high tendency to lose the solvent molecules and we found an interaction energy value of +2.28 eV, followed by complex **5** with benzonitrile (IE = +0.33 eV) and then complex **3** with toluene molecules (IE = +0.09 eV). The latter presents the smallest interaction energy value of the four solvates. It is noteworthy that the value of the interaction energy given could be overestimated for complex **2**, probably due to the complex electronic interactions and the limitlessness of the pseudopotential approach.

In view of these results, it could be argued that the starting supramolecular complex **1** displays a high tendency to interact with solvent molecules due to the opened structural arrangement with large voids but, at the same time, this also facilitates the spontaneous loss of the solvent molecules under ambient conditions, leading to facile recovery of complex **1**.

Conclusions

In view of the results obtained throughout this work, it can be concluded that compound **1** presents a vapochromic behaviour by which it lodges small organic solvent molecules in the holes in its crystalline structure, with an evident change in both the colour of the compound and its luminescence. These changes also affect the homo- and heterometallic distances presented by its crystal structures. Moreover, the theoretical study carried out on all of them reveals that the origin of the emission is not affected in any case by the solvent molecules inside them, but by charge transfers from gold centres and/or perhalophenyl ligands to the neutral terpyridine ligand.

Experimental section

General

$[Au_2Ag_2(C_6F_5)_4(Et_2O)_2]_n$ was prepared according to literature methods.[13d]

Materials and physical measurements

Infrared spectra were recorded in the 3500–450 cm^{-1} range on a PerkinElmer FT-IR Spectrum Two with a UATR (Single Reflection Diamond) accessory. ^1H and ^{19}F NMR spectra were recorded on a Bruker Avance 300 instrument in deuterated DMSO solutions at room temperature. Chemical shifts are quoted relative to $SiMe_4$ (^1H external) and $CFCl_3$ (^{19}F external). C, H, and N analyses were carried out with a C.E. Instrument EA-1110 CHNSO microanalyser. The MALDI mass spectra were registered on a Microflex Bruker spectrometer using DIT (dithranol) and DCTB (T-2-(3-(4-*t*-butylphenyl)-2-methyl-2-propenylidene)-malononitrile) as the matrix. The *m*/*z* values are obtained for the higher peak in the isotopic pattern. Absorption spectra in solution were recorded on a Hewlett-Packard 8453 diode array UV–visible spectrophotometer. Diffuse reflectance UV–vis spectra of pressed powder samples diluted with silica were recorded on a Shimadzu UV-3600 spectrophotometer with a Harrick Praying Mantis accessory and recalculated following the Kubelka–Munk function. Excitation and emission spectra in the solid state were recorded with an Edinburgh FLS 1000 fluorescence spectrometer. Luminescence lifetime was measured on an Edinburgh FLS 1000 fluorescence spectrometer. For measurements at RT, this equipment was used with a supercontinuum White Light Laser SuperK Extreme NKT Photonics. Time-resolved phosphorescence decay measurements at 77 K were analysed using numerical reconvolution. To do this, the corresponding instrumental response function (IRF) is necessary to detect the scattered light from the sample. Quantum yields were measured in

the solid state using an N-M01 integrating sphere with excitation at 560 nm on an Edinburgh FLS 1000 fluorescence spectrometer.

Synthesis

[{Au(C$_6$F$_5$)$_2$}$_2${Pb(terpy)(NCMe)$_2$}]$_n$ (2). A solution of **1** (0.088 g, 0.4 mmol) in acetonitrile (10 mL) was stirred for 10 min. Evaporation of the solvent to dryness gave a yellow solid in an almost quantitative yield. ^{1}H NMR (300 MHz, [D$_6$]-DMSO, 298 K), δ 8.69 (m, 2H, H$_1$), 8.59 (m, 2H, H$_4$), 8.41 (d, 2H, H$_5$, ^3JH$_5$–H$_6$ = 7.77 Hz), 8.07 (m, 1H, H$_6$), 7.98 (td, 2H, H$_3$, ^3J(H$_3$–H$_2$)–^3J(H$_3$–H$_4$) = 7.70 Hz, ^4J(H$_3$–H$_1$) = 1.78 Hz), 7.47 (ddd, 2H, H$_2$, ^3J(H$_2$–H$_3$) = 7.44 Hz, ^3J(H$_2$–H$_1$) = 4.72 Hz, ^4J(H$_2$–H$_4$) = 1.04 Hz), 2.02 (s, 3H, CH$_3$) ppm. ^{19}F NMR (282 MHz, [D$_6$]-DMSO, 298 K) δ −114.6 (m, 4F, F$_o$), −161.5 (t, 2F, F$_p$, ^3J(F$_p$–F$_m$) = 21.4 Hz), −162.8 (m, 4F, F$_m$) ppm. FT-IR (UATR): ν = 770, 955, 1471 cm^{-1} (Au–C$_6$F$_5$), ν = 1506 cm^{-1} (C═N) (Fig. 8), ν = 2247 cm^{-1} (acetronitrile). MALDI(+): *m*/*z* (%): 972 (100) [AuPb(C$_6$F$_5$)$_2$(terpy)]$^+$; MALDI(−): *m*/*z* (%): 530 (100) [Au(C$_6$F$_5$)$_2$]$^-$; elemental analysis calcd (%) for C$_{43}$H$_{17}$Au$_2$F$_{20}$N$_5$Pb: C, 32.59; H, 1.08; N, 4.42. Found: C, 32.22; H, 1.01; N, 4.31. Λ_M (acetone): 226.5 K^{-1} cm^2 mol^{-1}.

{[{Au(C$_6$F$_5$)$_2$}$_2${Pb(terpy)}]·toluene}$_n$ (3). A solution of **1** (0.088 g, 0.4 mmol) in toluene (10 mL) was stirred for 10 min. Evaporation of the solvent to dryness gave a dark green solid in an almost quantitative yield. ^{1}H NMR (300 MHz, [D$_6$]-DMSO, 298 K), δ 8.75 (m, 2H, H$_1$), 8.65 (m, 2H, H$_4$), 8.47 (d, 2H, H$_5$, ^3JH$_5$–H$_6$ = 7.75 Hz), 8.12 (m, 1H, H$_6$), 8.03 (td, 2H, H$_3$, ^3JH$_3$–H$_2$–^3JH$_3$–H$_4$ = 7.63 Hz, ^4JH$_3$–H$_1$ = 1.79 Hz), 7.52 (ddd, 2H, H$_2$, ^3JH$_2$–H$_3$ = 7.49 Hz, ^3JH$_2$–H$_1$ = 4.82 Hz, ^4JH$_2$–H$_4$ = 1.18 Hz), 7.26 (m, 2H, CH), 7.18 (m, 3H, CH), 2.31 (s, 3H, CH$_3$) ppm. ^{19}F NMR (282 MHz, [D$_6$]-DMSO, 298 K) δ −114.6 (m, 4F, F$_o$), −161.5 (t, 2F, F$_p$, ^3JF$_p$–F$_m$ = 21.4 Hz), −162.8 (m, 4F, F$_m$) ppm. FT-IR (UATR): ν = 767, 958, 1469 cm^{-1} (Au–C$_6$F$_5$), ν = 1506 cm^{-1} (C═N). MALDI(+): *m*/*z* (%): 972 (100) [AuPb(C$_6$F$_5$)$_2$(terpy)]$^+$; MALDI(−): *m*/*z* (%): 530 (100) [Au(C$_6$F$_5$)$_2$]$^-$; elemental analysis calcd (%) for C$_{46}$H$_{19}$Au$_2$F$_{20}$N$_3$Pb: C, 34.64; H, 1.20; N, 2.64. Found: C, 34.41; H, 1.04; N, 2.83. Λ_M (acetone): 215.7 K^{-1} cm^2 mol^{-1}.

[{Au(C$_6$F$_5$)$_2$}$_2${Pb(terpy)(THF)}]·THF (4). A solution of **1** (0.088 g, 0.4 mmol) in THF (10 mL) was stirred for 10 min. Evaporation of the solvent to dryness gave a yellow solid in an almost quantitative yield. ^{1}H NMR (300 MHz, [D$_6$]-DMSO, 298 K), δ 8.75 (m, 2H, H$_1$), 8.63 (m, 2H, H$_4$), 8.48 (d, 2H, H$_5$, ^3JH$_5$–H$_6$ = 7.85 Hz), 8.16 (m, 1H, H$_6$), 8.05 (td, 2H, H$_3$, ^3JH$_3$–H$_2$–^3JH$_3$–H$_4$ = 7.71 Hz, ^4JH$_3$–H$_1$ = 1.68 Hz), 7.55 (ddd, 2H, H$_2$, ^3JH$_2$–H$_3$ = 7.26 Hz, ^3JH$_2$–H$_1$ = 4.93 Hz, ^4JH$_2$–H$_4$ = 0.76 Hz), 3.60 (m, 2H, CH$_2$), 1.76 (m, 2H, CH$_2$) ppm. ^{19}F NMR (282 MHz, [D$_6$]-DMSO, 298 K) δ −114.6 (m, 4F, F$_o$), −161.7 (t, 2F, F$_p$, ^3JF$_p$–F$_m$ = 21.1 Hz), −163.0 (m, 4F, F$_m$) ppm. FT-IR (UATR): ν = 769, 951, 1472 cm^{-1} (Au–C$_6$F$_5$), ν = 1505 cm^{-1} (C═N). MALDI(+): *m*/*z* (%): 972 (100) [AuPb(C$_6$F$_5$)$_2$(terpy)]$^+$; MALDI(−): *m*/*z* (%): 530 (100) [Au(C$_6$F$_5$)$_2$]$^-$; elemental analysis calcd (%) for C$_{47}$H$_{27}$Au$_2$O$_2$F$_{20}$N$_3$Pb: C, 34.28; H, 1.65; N, 2.55. Found: C, 34.45; H, 1.71; N, 2.66. Λ_M (acetone): 214.8 K^{-1} cm^2 mol^{-1}.

Crystallography

Crystals were mounted in inert oil on a MiteGen MicroMounts™ and transferred to the cold gas stream of a Nonius Kappa CCD (**3**) or in a Bruker APEX-II CCD diffractometer (**2** and **4**) equipped with an Oxford Instruments low-temperature attachment. Data were collected using monochromated Mo Kα radiation (λ = 0.71073 Å). Scan type: ω and ϕ. Absorption corrections: empirical (**2** and **3**) or semi-empirical (**4**). In spite of having tested several absorption correction types in order to choose the best one to minimize them, the crystal structure of complex **2** contains residual peaks and holes larger than desired, although they are close to the heavy atoms. This fact is probably due to the number of heavy atoms and the high value of the absorption coefficient in these structures. The structures were solved with the XT structure solution program using Intrinsic Phasing and refined with the ShelXL refinement package using Least Squares minimization (**2** and **4**) or by direct methods (**3**) and refined on F^2 using the program SHELXL-97.[23] The non-coordinated THF molecule in **4** is disordered over two different positions (60 : 40). All non-hydrogen atoms, except those of the non-coordinated THF molecule in **4**, were refined anisotropically. Hydrogen atoms were included using a riding model. CCDC 2266131–2266133† contain the supplementary crystallographic data for this paper.

Computational details

All calculations were performed using the Gaussian 09 suite of programs[24] using DFT-BP86 level of theory.[25]

We have performed single-point calculations on all model systems at the DFT-D3/BP86 level, including the empirical dispersion correction by Grimme *et al.*[26] This level of theory has been proven to represent noncovalent interactions at lower computational cost. For these calculations, the corresponding def2-TZVP basis sets were used.[27]

Periodic DFT calculations were based on the plane augmented wave (PAW) method with pseudopotentials.[28] This methodology is implemented in the Quantum Espresso package.[29] Plane waves and basis sets were expanded with an energy cutoff equal to 70 Ry. The periodic cell boundaries and the lattice constants were taken from the experimental data and are depicted in Table 1. For single point energy calculations, a 4 × 4 x 4 *k*-point Monkhorst Pack-Mesh is used in the first Brillouin zone. For all systems, the energy convergence should reach a value equal to 10^{-7} eV, and the convergence in the forces should reach a threshold of 0.01 eV A^{-1}. In all the calculations, GGA-PBE was used to treat the exchange–correlation potential.[30]

Conflicts of interest

There are no conflicts to declare.

Acknowledgements

We gratefully acknowledge DGI MICINN/FEDER (project number PID2022-139739NB-I00 (AEI/FEDER, UE)) and "ERDF A way of making Europe". S. M. also acknowledges MINECO for an FPI grant. A. G. E.-H. thanks the MU and the EU-NextGeneration program for a Maria Zambrano post-doctoral scholarship.

References

1 V. W.-W. Yam, V. K.-M. Au and S. Yu-Lut, Leung. Light-Emitting Self-Assembled Materials Based on d^8 and d^{10} Transition Metal Complexes, *Chem. Rev.*, 2015, **115**, 7589–7728.

2 *Modern Supramolecular Gold Chemistry: Gold–Metal Interactions and Applications*, ed. A. Laguna, Wiley-VCH, Weinheim, Germany, 2008, p. 181.

3 See for example: (*a*) M. Gil-Moles, M. C. Gimeno, J. M. López-de-Luzuriaga, M. Monge and D. Pascual, Tailor Made Luminescent Polymers through Unusual Metallophilic Interaction Arrays Au···Au···Ag···Ag, *Inorg. Chem.*, 2017, **56**, 9281–9290; (*b*) M. E. Olmos, A. Schier and H. Schmidbaur, 2-(Diphenylphosphino)pyridine as an Ambidentate Ligand in Homo- and Hetero-binuclear Complexes of Copper, Silver, and Gold, *Z. Naturforsch., B: J. Chem. Sci.*, 1997, **52**, 203–208; (*c*) V. J. Catalano and A. L. Moore, Mono-, Di-, and Trinuclear Luminescent Silver (I) and Gold(I) N-Heterocyclic Carbene Complexes Derived from the Picolyl-Substituted Methylimidazolium Salt: 1-Methyl-3-(2-pyridinylmethyl)-1H-imidazolium Tetrafluoroborate, *Inorg. Chem.*, 2005, **44**, 6558–6566; (*d*) Q. M. Wang, Y. A. Lee, O. Crespo, J. Deaton, C. Tang, H. J. Gysling, M. C. Gimeno, C. Larraz, M. D. Villacampa, A. Laguna and R. Eisenberg, Intensely Luminescent Gold (I)-Silver(I) Cluster Complexes with Tunable Structural Features, *J. Am. Chem. Soc.*, 2004, **126**, 9488–9489.

4 See for example: (*a*) R. Donamaría, E. J. Fernández, J. M. López-de-Luzuriaga, M. Monge, M. E. Olmos, D. Pascual and M. Rodríguez-Castillo, New Au(I)–Cu(I) heterometallic complexes: the role of bridging pyridazine ligands in the presence of unsupported metallophilic interactions, *Dalton Trans.*, 2017, **46**, 10941–10949; (*b*) M. J. Calhorda, C. Ceamanos, O. Crespo, M. C. Gimeno, A. Laguna, C. Larraz, P. D. Vaz and M. D. Villacampa, Heteropolynuclear Gold Complexes with Metallophilic Interactions: Modulation of the Luminescent Properties, *Inorg. Chem.*, 2010, **49**, 8255–8269; (*c*) E. J. Fernández, A. Laguna, J. M. López-de-Luzuriaga, M. Monge, M. Montiel, M. E. Olmos and M. Rodríguez-Castillo, Unsupported Au(I)···Cu(I) interactions: influence of nitrile ligands and aurophilicity on the structure and luminescence, *Dalton Trans.*, 2009, **36**, 7509–7518.

5 See for example: (*a*) A. Burini, J. P. Fackler, Jr., R. Galassi, T. A. Grant, M. A. Omary, M. A. Rawashdeh-Omary, B. R. Pietroni and R. J. Staples, Supramolecular Chain Assemblies Formed by Interaction of a π Molecular Acid Complex of Mercury with π-Base Trinuclear Gold Complexes, *J. Am. Chem. Soc.*, 2000, **122**, 11264–11265; (*b*) J. M. López-de-Luzuriaga, M. Monge, M. E. Olmos and D. Pascual, Experi-mental and Theoretical Comparison of the Metallophilicity between d^{10}–d^{10} Au^{I}–Hg^{II} and d^8–d^{10} Au^{III}–Hg^{II} Interactions, *Inorg. Chem.*, 2014, **53**, 1275–1277; (*c*) T. Lasanta, J. M. López-de-Luzuriaga, M. Monge, M. E. Olmos and D. Pascual, Synthesis of the molecular amalgam $[\{AuHg_2(o\text{-}C_6F_4)_3\}\{Hg_3(o\text{-}C_6F_4)_3\}]^-$: a rare example of a heterometallic homoleptic metallacycle, *Dalton Trans.*, 2016, **45**, 6334–6338.

6 See for example: (*a*) R. Donamaría, M. C. Gimeno, V. Lippolis, J. M. López-de-Luzuriaga, M. Monge and M. E. Olmos, Tuning Au(I)···Tl(I) Interactions via Mixed ThiaAza Macrocyclic Ligands: Effects on the Structural and Luminescence Properties, *Inorg. Chem.*, 2017, **56**, 12551–12563; (*b*) V. J. Catalano, B. L. Bennett, H. M. Kar and B. C. Noll, Synthesis and Characterization of Trigonal Gold (I) Cage Complexes: Luminescent Metallocryptates Encapsulating Tl(I) and Na^+ Ions, *J. Am. Chem. Soc.*, 1999, **121**, 10235–10236.

7 (*a*) S. H. Lim, M. M. Olmstead, J. C. Fettinger and A. L. Balch, Polymorphs and Aurophilic Interactions in Colourless Crystals of Au_2(μ-1,2 bis-(diphenylarsino)ethane) X_2, (X = Cl, Br, I), *Inorg. Chem.*, 2012, **51**, 1925–1932; (*b*) A. L. Balch, Polymorphism and luminescent behaviour of linear, two-coordinate gold(I) complexes, *Gold Bull.*, 2004, **37**, 45–50.

8 E. J. Fernández, M. C. Gimeno, A. Laguna, J. M. López-de-Luzuriaga, M. Monge, P. Pyykkö and D. Sundholm, Luminescent Characterization of Solution Oligomerization Process Mediated Gold-Gold Interactions. DFT Calculations on $[Au_2Ag_2R_4L_2]_n$ Moieties, *J. Am. Chem. Soc.*, 2000, **122**, 7287–7293.

9 W. C. McCrone, *Physics and Chemistry of the Organic Solid State*, ed. D. Fox, M. M. Labels and A. Weissberger, Interscience, London, 1965, vol. 2, pp. 725–767.

10 H. G. Brittain, Polymorphism and solvatomorphism 2006, *J. Pharm. Sci.*, 2008, **97**, 3611–3636.

11 M. Asaoka, Y. Kitagawa, R. Teramoto, K. Miyagi, Y. Natori and M. Nakano, Origin of Solvent-independent Optical Property of Unsubstituted BODIPY Revisited, *Chem. Lett.*, 2017, **46**, 1–3.

12 M. A. Mansour, W. B. Connick, R. J. Lachicotte, H. J. Gysling and R. Eisenberg, Linear Chain Au(I) Dimer Compounds as Environmental Sensors: A Luminescent Switch for the Detection of Volatile Organic Compounds, *J. Am. Chem. Soc.*, 1998, **120**, 1329–1330.

13 (*a*) I. O. Koshevoy, Y.-C. Chang, A. J. Karttunen, M. Haukka, T. Pakkanen and P.-T. Chou, Modulation of Metallophilic Bonds: Solvent-Induced Isomerization and Luminescence Vapochromism of a Polymorphic Au-Cu Cluster, *J. Am. Chem. Soc.*, 2012, **134**, 6564–6567; (*b*) E. J. Fernández, J. M. López-de-Luzuriaga, M. Monge, M. E. Olmos, J. Pérez,

A. Laguna, A. A. Mohamed and J. P. Facker, Jr., {Tl[Au(C_6Cl_5)$_2$]}$_n$: A Vapochromic Complex, *J. Am. Chem. Soc.*, 2003, **125**, 2022–2023; (*c*) E. J. Fernández, J. M. López-de-Luzuriaga, M. Monge, M. Montiel, A. A. Mohamed and J. P. Facker, A Detailed Study of the Vapochromic Behaviour of {Tl[Au(C_6Cl_5)$_2$]}$_n$, *Inorg. Chem.*, 2004, **43**, 3573–3581; (*d*) E. J. Fernández, J. M. López-de-Luzuriaga, M. Monge, M. E. Olmos, R. C. Puelles, A. Laguna, A. A. Mohamed and J. P. Facker, Jr., *Inorg. Chem.*, 2008, **47**, 8069–8076; (*e*) E. J. Fernández, A. Laguna, J. M. López-de-Luzuriaga, M. E. Olmos and R. C. Puelles, *Z. Naturforsch., B: J. Chem. Sci.*, 2009, **64**, 1500–1512; (*f*) T. Lasanta, M. E. Olmos, A. Laguna, J. M. López-de-Luzuriaga and P. Naumov, *J. Am. Chem. Soc.*, 2011, **133**, 16358–16361; (*g*) J. Lefebvre, R. J. Batchelor and D. B. Leznoff, Cu[Au-(CN)$_2$]$_2$(DMSO)$_2$: Golden Polymorphs That Exhibit Vapochromic Behaviour, *J. Am. Chem. Soc.*, 2004, **126**, 16117–16125; (*h*) J. Lefebvre, J. L. Korčok, M. J. Katz and D. B. Lenznoff, Vapochromic Behaviour of M[Au(CN)$_2$]$_2$-Based Coordination Polymers (M = Co, Ni), *Sensors*, 2012, **12**, 3669–3692; (*i*) J. Lefebvre, F. Callaghan, M. J. Katz, J. E. Sonier and D. B. Leznoff, A New Basic Motif in Cyanometallate Coordination Polymers: Structure and Magnetic Behaviour of M(μ-OH$_2$)$_2$[Au(CN)$_2$]$_2$ (M = Cu, Ni), *Chem. – Eur. J.*, 2006, **12**, 6748–6761; (*j*) J. Lefebvre, P. Tyagi, S. Trudel, V. Pacradouni, C. Kaiser, J. E. Sonier and D. B. Leznoff, Magnetic Frustration and Spin Disorder in Isostructural M(μ-OH$_2$)$_2$[Au(CN)$_2$]$_2$ (M = Mn, Fe, Co) Coordination Polymers Containing Double Aqua-Bridged Chains: SQUID and μSR Studies, *Inorg. Chem.*, 2009, **48**, 55–67; (*k*) M. J. Katz, T. Ramnial, H. Z. Yu and D. B. Leznoff, Polymorphism of Zn[Au(CN)$_2$]$_2$ and Its Luminescent Sensory Response to NH3 Vapour, *J. Am. Chem. Soc.*, 2008, **130**, 10662–10673; (*l*) B. R. Varju, J. S. Ovens and D. B. Leznoff, Mixed Cu(I)/Au(I) Coordination Polymers as Reversible Turn-on Vapoluminescent Sensors for Volatile Thioethers, *Chem. Commun.*, 2017, **53**, 6500–6503; (*m*) A. Luquin, C. Bariáin, E. Vergara, E. Cerrada, J. Garrido, I. R. Matias and M. Laguna, New Preparation of Gold–Silver Complexes and Optical Fibre Environmental Sensors Based on Vapochromic [Au$_2$Ag$_2$(C_6F_5)$_4$(phen)$_2$]$_n$, *Appl. Organomet. Chem.*, 2005, **19**, 1232–1238; (*n*) R. Usón, A. Laguna, M. Laguna, P. G. Jones and G. M. Sheldrick, Synthesis and Reactivity of Bimetallic Au–Ag Complexes. X-Ray Structure of a Chain Polymer Containing the Moiety ⋯(F_5C_6)$_2$Au(μ-AgSC_4H_8)$_2$Au(C_6F_5)$_2$⋯, *J. Chem. Soc., Chem. Commun.*, 1981, 1097–1098; (*o*) R. Usón, A. Laguna, M. Laguna, B. R. Manzano, P. G. Jones and G. M. Sheldrick, Synthesis and Reactivity of Bimetallic Au-Ag Polyfluorophenyl Complexes; Crystal and Molecular Structures of [{AuAg(C_6F_5)$_2$(SC_4H_8)}$_n$] and [{AuAg(C_6F_5)$_2$(C_6H_6)}$_n$], *Dalton Trans.*, 1984, 285–292; (*p*) E. J. Fernández, M. C. Gimeno, A. Laguna, J. M. López-de-Luzuriaga, M. Monge, P. Pyykkö and D. Sundholm, Luminescent Characterization of Solution Oligomerization Process Mediated Gold-Gold Interactions. DFT Calculations on [Au$_2$Ag$_2$R$_4$L$_2$]$_n$ Moieties, *J. Am. Chem. Soc.*, 2000, **122**, 7287–7293; (*q*) M. Laguna, C. Bariáin, J. Garrido, I. R. Matías and I. Romeo, *Spanish Patent*, E-99-02862, 1999; C. Bariáin, J. Garrido, I. R. Matias and I. Romeo, *European Patent*, PCT/ES00/00485, 2000; (*r*) M. Laguna, J. Garrido and I. Romeo, *Spanish Patent*, 2151424, 2001; (*s*) C. Bariáin, I. R. Matías, I. Romeo, J. Garrido and M. Laguna, Detection of Volatile Organic Compound Vapours by Using a Vapochromic Material on a Tapered Optical Fiber, *Appl. Phys. Lett.*, 2000, **77**, 2274–2276; (*t*) C. Bariáin, I. R. Matías, I. Romeo, J. Garrido and M. Laguna, Behavioural Experimental Studies of a Novel Vapochromic Material Towards Development of Optical Fiber Organic Compounds Sensor, *Sens. Actuators, B*, 2001, **76**, 25–31; (*u*) C. Bariáin, I. R. Matías, C. Fdez-Valdivielso, C. Elosúa, A. Luquin, J. Garrido and M. Laguna, Optical Fibre Sensors Based on Vapochromic Gold Complexes for Environmental Applications, *Sens. Actuators, B*, 2005, **108**, 535–541; (*v*) S. C. Terrones, C. E. Aguado, C. Bariáin, A. S. Carretero, I. R. M. Maestro, A. F. Gutiérrez, A. Luquin, J. Garrido and M. Laguna, Volatile-Organic-Compound Optic Fiber Sensor Using a Gold-Silver Vapochromic Complex, *Opt. Eng.*, 2006, **45**, 044401–044407; (*w*) C. Elosua, I. Matías, C. Bariain and F. Arregui, Development of an In-Fiber Nanocavity Towards Detection of Volatile Organic Gases, *Sensors*, 2006, **6**, 578–592; (*x*) Z. Lei, S. S. Chang and Q. W. Wang, Vapochromic Gold(I)-Silver(I) Cluster Protected by Alkynyl and Phosphine Ligands, *Eur. J. Inorg. Chem.*, 2017, **2017**, 5098–5102; (*y*) L. Q. Mo, J. H. Jia, L. J. Sun and Q. M. Wang, Solvent-Induced Intercluster Rearrangements and the Reversible Luminescence Responses in Sulfide Bridged Gold(I)-Silver(I) Clusters, *Chem. Commun.*, 2012, **48**, 8691–8693; (*z*) S. H. Lim, M. M. Olmstead and A. L. Balch, Molecular Accordion: Vapoluminescence and Molecular Flexibility in the Orange and Green Luminescent Crystals of the Dimer, Au$_2$(μ-bis-(diphenylphosphino)ethane)$_2$Br$_2$, *J. Am. Chem. Soc.*, 2011, **133**, 10229–10238.

14 (*a*) K. R. England, S. H. Lim, L. M. C. Luong, M. M. Olmstead and A. L. Balch, Vapoluminescent Behaviour and the Single-Crystal-to-Single-Crystal Transformations of Chloroform Solvates of [Au$_2$(μ-1,2-bis(diphenylarsino)ethane)$_2$](AsF_6)$_2$, *Chem. – Eur. J.*, 2019, **25**, 874–878; (*b*) M. S. Jiang, Y. H. Tao, Y. W. Wang, C. Lu, D. J. Young, J. P. Lang and Z. G. Ren, Reversible Solid-State Phase Transitions Between Au-P Complexes Accompanied by Switchable Fluorescence, *Inorg. Chem.*, 2020, **59**, 3072–3078; (*c*) A. Chu, F. K. W. Hau, L. Y. Yao and V. W. W. Yam, Decanuclear Gold(I) Sulfido Pseudopolymorphs Displaying Stimuli-Responsive RGBY Luminescence Changes, *ACS Mater. Lett.*, 2019, **1**, 277–284; (*d*) Y. F. Hsu, T. W. Wu, Y. H. Kang, C. Y. Wu, Y. H. Liu, S. M. Peng, K. V. Kong and J. S. Yang, Porous Supramolecular Assembly of Pentiptycene-Containing Gold(I) Complexes: Persistent Excited-State Aurophilicity and Inclusion-Induced Emission Enhancement, *Inorg. Chem.*, 2022, **61**, 11981–

11991; (*e*) J. A. Pells, D. Guan and D. B. Leznoff, Heterobimetallic Ln(III)-Containing Materials Based on One-Dimensional Aurophilic Chains of Gold(I) Dithiolate Dimers and Their Vapochromic Response to DMF, *Eur. J. Inorg. Chem.*, 2022, e202200049; (*f*) Y. F. Hsu, S. Y. Chen, S. Maity, Y. H. Liu, S. M. Peng and J. S. Yang, A polymorphic pentiptycene-containing gold(I) isocyanide complex: solvent- and conformation-dependent supramolecular luminescence, *Dalton Trans.*, 2020, **49**, 15602–15606; (*g*) L. M. C. Luong, C. D. Lowe, A. V. Adams, V. Moshayedi, M. M. Olmstead and A. L. Balch, Seeing luminescence appear as crystals crumble. Isolation and subsequent self-association of individual $[(C_6H_{11}NC)_2Au]^+$ ions in crystals, *Chem. Sci.*, 2020, **11**, 11705–11713; (*h*) L. M. C. Luong, M. A. Malwitz, V. Moshayedi, M. M. Olmstead and A. L. Balch, Role of Anions and Mixtures of Anions on the Thermochromism, Vapochromism, and Polymorph Formation of Luminescent Crystals of a Single Cation, $[(C_6H_{11}NC)_2Au]^+$, *J. Am. Chem. Soc.*, 2020, **142**, 5689–5701; (*i*) S. Nayeri, S. Jamali, A. Jamjah and H. Samouei, Tetranuclear Au_2Cu_2 Clusters with Butterfly- and Planar-Shaped Metal Cores: Strong Rigidochromism Induced by Jahn–Teller Distortion in Two-Coordinated Gold(I) Centres, *Inorg. Chem.*, 2019, **58**, 12122–12131; (*j*) S. Ibáñez and E. Peris, Chemically Tunable Formation of Different Discrete, Oligomeric, and Polymeric Self-Assembled Structures from Digold Metallotweezers, *Chem. – Eur. J.*, 2018, **24**, 8424–8431.

15 (*a*) R. Echeverría, J. M. López-de-Luzuriaga, M. Monge and M. E. Olmos, The gold(I)···lead(II) interaction: a relativistic connection, *Chem. Sci.*, 2015, **6**, 2022–2026; (*b*) R. Echeverría, J. M. López-de-Luzuriaga, M. Monge, S. Moreno and M. E. Olmos, New Insights into the Au(I)···Pb(II) Closed-Shell Interaction: Tuning of the Emissive Properties with the Intermetallic Distance, *Inorg. Chem.*, 2016, **20**, 10523–10534; (*c*) R. Echeverría, J. M. López-de-Luzuriaga, M. Monge, S. Moreno, M. E. Olmos and M. Rodríguez-Castillo, Lead encapsulation by a golden clamp through multiple electrostatic, metallophilic, hydrogen bonding and weak interactions, *Chem. Commun.*, 2018, **3**, 295–298.

16 J. M. López-de-Luzuriaga, M. Monge, S. Moreno, M. E. Olmos and M. Rodríguez-Castillo, Rational Assembly of Metallophilic Gold(I)–Lead(II) and Gold(I)–Gold(I) Puzzle Pieces, *Angew. Chem., Int. Ed.*, 2021, **60**, 640–644.

17 S. Moreno, N. Casati, M. Rodríguez-Castillo, M. Monge, M. E. Olmos and J. M. López-de-Luzuriaga, Switching on/off of a solvent coordination in a Au(I)-Pb(II) complex: high-pressure and temperature as external stimuli, *Inorg. Chem.*, 2023, **62**, 10307–10316.

18 S. Wang, G. Garzon, C. King, J.-C. Wang and J. P. Fackler, Jr., Luminescent extended one-dimensional heterobimetallic chain compounds with relativistic metal-metal bonds. Synthesis, crystal structures, and spectroscopic studies of $AuTl(MTP)_2$ a nd $Au_2Pb(MTP)_4$ (MTP = $[CH_2P(S)Ph_2]^-$, *Inorg. Chem.*, 1989, **28**, 4623–4629.

19 https://www.webelements.com/.

20 S. Alvarez, A cartography of the van der Waals territories, *Dalton Trans.*, 2013, **42**, 8617–8636.

21 L. Shimoni-Livny, J.-P. Glusker and C. W. Bock, Lone Pair Func-tionality in Divalent Lead Compounds, *Inorg. Chem.*, 1998, **37**, 1853–1867.

22 (*a*) A. Morsali, Syntheses and Characterization of Two New Lead(II) Acetate Complexes, $Pb(L)(CH_3COO)_2$, L = 2,2′: 6′,2″-Terpyridine (tpy) and 2,4,6-Tris(2-pyridyl)-1,3,5-Triazine (trz), Crystal Structure of $Pb(tpy)(CH_3COO)_2$, *Z. Naturforsch., B: J. Chem. Sci.*, 2004, **59**, 1039–1044; (*b*) N. Noshiranzadeh, A. Ramazani, A. Morsali, A. D. Hunter and M. Zeller, 4′-(4-Pyridyl)-2,2′: 6′,2″-terpyridine as ligand in the lead(II) complexes, [Pb(pyterpy)(MeOH)I_2]·MeOH and $[Pb(pyterpy)(\mu\text{-AcO})]_2(ClO_4)_2$, *Inorg. Chim. Acta*, 2007, **360**, 3603–3609.

23 G. M. Sheldrick, *SHELXL97, Program for Crystal Structure Refinement*, University of Göttingen, Germany, 1997.

24 M. J. Frisch, G. W. Trucks, H. B. Schlegel, G. E. Scuseria, M. A. Robb, J. R. Cheeseman, G. Scalmani, V. Barone, G. A. Petersson, H. Nakatsuji, X. Li, M. Caricato, A. Marenich, J. Bloino, B. G. Janesko, R. Gomperts, B. Mennucci, H. P. Hratchian, J. V. Ortiz, A. F. Izmaylov, J. L. Sonnenberg, D. Williams-Young, F. Ding, F. Lipparini, F. Egidi, J. Goings, B. Peng, A. Petrone, T. Henderson, D. Ranasinghe, V. G. Zakrzewski, J. Gao, N. Rega, G. Zheng, W. Liang, M. Hada, M. Ehara, K. Toyota, R. Fukuda, J. Hasegawa, M. Ishida, T. Nakajima, Y. Honda, O. Kitao, H. Nakai, T. Vreven, K. Throssell, J. A. Montgomery, Jr., J. E. Peralta, F. Ogliaro, M. Bearpark, J. J. Heyd, E. Brothers, K. N. Kudin, V. N. Staroverov, T. Keith, R. Kobayashi, J. Normand, K. Raghavachari, A. Rendell, J. C. Burant, S. S. Iyengar, J. Tomasi, M. Cossi, J. M. Millam, M. Klene, C. Adamo, R. Cammi, J. W. Ochterski, R. L. Martin, K. Morokuma, O. Farkas, J. B. Foresman and D. J. Fox, *Gaussian 09, Revision A.1*, Gaussian, Inc., Wallingford CT, 2009.

25 (*a*) A. D. Becke, Density–functional thermochemistry. I. The effect of the exchange–only gradient correction, *J. Chem. Phys.*, 1992, **96**, 2155–2160; (*b*) A. D. Becke, Density–functional thermochemistry. III. The role of exact exchange, *J. Chem. Phys.*, 1993, **98**, 5648–5652; (*c*) C. Lee, W. Yang and R. G. Parr, Development of the Colle-Salvetti correlation-energy formula into a functional of the electron density, *Phys. Rev. Lett.*, 1998, **B37**, 785–789.

26 S. Grimme, J. Antony, S. Ehrlich and H. Krieg, A consistent and accurate ab initio parametrization of density functional dispersion correction (DFT-D) for the 94 elements H-Pu, *J. Chem. Phys.*, 2010, **132**, 1–19.

27 F. Weigend and R. Ahlrichs, Balanced basis sets of split valence, triple zeta valence and quadruple zeta valence quality for H to Rn: Design and assessment of accuracy, *Phys. Chem. Chem. Phys.*, 2005, **7**, 3297–3305.

28 P. E. Blöchl, Projector augmented-wave method, *Phys. Rev. B: Condens. Matter Mater. Phys.*, 1994, **50**, 17953.

29 P. Giannozzi, O. Andreussi, T. Brumme, O. Bunau, M. B. Nardelli, M. Calandra, R. Car, C. Cavazzoni,

D. Ceresoli, M. Cococcioni, N. Colonna, I. Carnimeo, A. D. Corso, S. de Gironcoli, P. Delugas, R. A. DiStasio Jr., A. Ferretti, A. Floris, G. Fratesi, G. Fugallo, R. Gebauer, U. Gerstmann, F. Giustino, T. Gorni, J. Jia, M. Kawamura, H.-Y. Ko, A. Kokalj, E. Küçükbenli, M. Lazzeri, M. Marsili, N. Marzari, F. Mauri, N. L. Nguyen, H.-V. Nguyen, A. Otero-de-la-Roza, L. Paulatto, S. Poncé, D. Rocca, R. Sabatini, B. Santra, M. Schlipf, A. P. Seitsonen, A. Smogunov, I. Timrov, T. Thonhauser, P. Umari, N. Vast, X. Wu and S. Baroni, Advanced capabilities for materials modelling with Quantum ESPRESSO, *J. Phys.: Condens. Matter*, 2017, **29**, 465901.

30 J. P. Perdew, K. Burke and M. Ernzerhof, Perdew, Burke, and Ernzerhof reply, *Phys. Rev. Lett.*, 1998, **80**, 891.